Journal of
Advanced Manufacturing Science and Technology
jamst@jamstjournal.com;jamst2020@126.com
www.jamstjournal.com

Transmission error prediction of spur gear and parameter optimization of tooth profile modification considering micro-contact of the tooth surface

Youcheng WANG [a], Jianhua LIU [a,b], Hao GONG [a,b,*], Yun LI [c], Xiao WANG [a], Lin LI [c]

[a] *School of Mechanical Engineering, Beijing Institute of Technology, Beijing 100081, China*
[b] *Tangshan Research Institute, Beijing Institute of Technology, Tangshan 063015, China*
[c] *Beijing Spacecraft Manufacturing Co., Ltd, Beijing 100094, China*

Received 28 October 2024; revised 22 November 2024; accepted 28 November 2024; available online 14 December 2024

Abstract: This study, which is based on Blending ensemble learning and a differential evolution algorithm, achieved the prediction of gear transmission error while considering micro-contact and the optimization of tooth profile modification. First, the micro-topography of the modified tooth surface was generated based on the conjugate gradient method. A modified spur gear model with a rough tooth surface was constructed, and its meshing process was simulated to obtain the static transmission error and calculate the peak-to-peak value. Second, on the basis of finite element modeling and simulation methods, the peak-to-peak values of the gear transmission error under different modification parameter conditions were obtained, and a dataset of 50 groups was constructed and divided into a training set and a test set. Eight single surrogate models were selected, and on the basis of the Blending ensemble learning strategy, base learners and meta-learners were optimized to construct a prediction model for the peak-to-peak value of the gear static transmission error. The differential evolution algorithm was employed to optimize modification parameters, minimizing the peak-to-peak value of static transmission error, with finite element simulation verifying the reliability of the optimization results. Research findings indicate that utilizing RF, SVR, GBM, and RBF as base learners and RBF as a meta-learner in the Blending ensemble learning model yields the highest prediction accuracy, achieving a Mean Absolute Percentage Error (MAPE) of 14.183%. This represents an average decrease in prediction error of 2.75% compared to single models. Furthermore, the peak-to-peak value of static transmission error for the gear with optimized modification parameters was 3.69 μm, a reduction of 23.19% compared to gears with randomly generated modification parameters, thereby validating the accuracy and reliability of the proposed method.

Keywords: Micro-topography; Tooth profile modification; Static transmission error; Ensemble learning; Differential evolution algorithm

1. Introduction

Involute spur gears are extensively employed in various mechanical equipment due to their superior manufacturing processes and transmission performance[1-4]. As gear transmission performance requirements continue to escalate and vibration and noise control during transmission become increasingly stringent, modification techniques have gained widespread acceptance to enhance gear mechanism performance. Micro-geometric parameters play a crucial role in reducing vibration and noise in gear mechanisms. Since these parameters are directly influenced by gear machining accuracy and specific operating conditions, determining optimal micro-geometric modification parameters remains a key challenge and research focus in gear structure optimization[5-7].

Numerical simulation methods, particularly the finite element method, are extensively utilized in gear structure optimization[8-11]. Notably, Wu et al. [12] developed an accurate gear model and employed the finite element method to determine the tooth profile modification (TPM) type and modification amount for a helical gear pair. Dynamic contact simulation experiments verified the effectiveness of their method, using vibration reduction as the evaluation criterion. Mei et al. [13] combined finite element analysis with a genetic algorithm to simulate the meshing process of spur gears and optimize modifications. Their study compared the impact of different modification methods on transmission error fluctuation, revealing that arc-shaped and parabolic modifications can reduce error fluctuation by 90%, thus enhancing transmission stability and efficiency. Furthermore, Chen et al.[14] investigated the effects of two tooth orientation modification methods (tooth end modification and symmetric crown modification) on the meshing performance of straight bevel gears using finite element analysis. The results indicate that tooth end modification is the optimal method for improv-

* Corresponding author. *E-mail address:* gonghao0220@bit.edu.cn(Hao GONG)
Peer review under responsibility of Editorial Committee of JAMST
DOI: 10.51393/j.jamst.2025018

ing meshing performance under various installation conditions, reducing transmission error fluctuation and enhancing contact stress and bending stress distribution.

The numerical simulation method's complexity and lengthy calculation time hinder efficient micro-geometric modification optimization of gears[15-18]. To address this, researchers employ meta-models (or surrogate models) to predict system responses and identify optimal micro-geometric modification parameters under specific working conditions, streamlining the design process. Korta and Mundo et al.[19] explored the applicability of Gaussian process, Shepard k-nearest neighbor, and polynomial meta-models in gear optimization via response surface methodology. Their study found optimal modification parameters that reduced peak transmission error and maximum contact stress while ensuring bending fatigue strength. Mohammed et al.[20] developed a modification optimization method using Gaussian regression to construct a meta-model for peak-to-peak transmission error, contact pressure, and tooth root stress, followed by multi-objective optimization using genetic algorithm. While these scholars relied on single models for transmission performance prediction and micro-modification optimization, single surrogate models have limitations in solving complex problems and generalization ability. To overcome these limitations, ensemble learning methods combining diverse learners have been proposed and applied to gear structure optimization and fault detection. Ensemble learning significantly enhances model generalization, reduces over-fitting risk, and improves robustness to noise and outliers. For instance, Liu et al.[21] combined ensemble learning and NSGA-II algorithm to optimize two-stage helical gear pairs in helical hydraulic rotary actuators, enhancing power density and fatigue life. Wang et al.[22] proposed a multi-criterion fault feature selection and heterogeneous ensemble learning classification scheme for planetary gearbox fault diagnosis, demonstrating its effectiveness and robustness through experiments.

The above research based on numerical simulation and surrogate model methods can obtain the optimal modification parameters for gear mechanisms under various working conditions. Additionally, researchers have explored the impact of tooth surface micro-contact on transmission performance, further refining gear optimization[23-25]. Zhao et al.[26] established a fractal contact model suitable for tooth surface contact and explored the influence of roughness on the time-varying meshing characteristics of gears (including the meshing stiffness, static transmission error, load distribution ratio, and contact stress). The results show that the micro-contact of the tooth surface significantly affects the transmission performance of gears, and the selection of gear micro-modification parameters should also consider the influence of micro-contact. However, existing methods do not consider the optimal tooth profile modification parameters under the influence of micro-contacts. Therefore, in this paper, considering the micro-contact of a specific rough gear surface, a transmission error prediction method based on Blending ensemble learning and a gear modification parameter optimization method based on a differential evolution algorithm are proposed, which rapidly predicts the peak-to-peak value of the gear static transmission error and optimizes the tooth profile modification parameters.

This study employed a multi-step approach to optimize gear modification parameters. Initially, a modified tooth surface model incorporating micro-topography was developed using the conjugate gradient method and tooth profile modification technique. Finite element modeling and meshing process simulation were then conducted to calculate the peak-to-peak value of static transmission error. Subsequently, finite element models were created under various modification parameters using the simulation modeling method, generating a dataset through simulation. Eight surrogate models, including random forest and support vector regression, were trained. The Blending ensemble learning strategy optimized base learners and meta-learners to construct an ensemble learning model for predicting peak-to-peak static transmission error. Finally, combining the optimal prediction model with the differential evolution algorithm, modification parameters minimizing peak-to-peak static transmission error under specific tooth surface roughness and operating conditions were determined. The finite element method verified the reliability of the optimization results.

2. Tooth surface modeling considering micro-topography and tooth profile modification

Involute gears typically exhibit a rough surface at the microscopic scale, characterized by numerous micro-convex structures, due to factors such as manufacturing methods, machining errors, and surface wear. During meshing, contact deformations of these micro-convex structures cause transmission error fluctuations, leading to significant vibrations and noise in gear mechanisms. This, in turn, affects gear system transmission performance. To mitigate vibrations and noise, micro-geometry profile modification techniques are widely employed. However, the selection of optimal modification parameters is crucial, as it substantially influences vibration and noise reduction efficacy. Achieving optimal tooth profile modification parameters for specific operating conditions and surface roughness requires accurate modeling of the gear surface, considering its micro-topography, as a prerequisite for effective tooth profile modification. This precise modeling enables the identification of optimal modification parameters, enhancing transmission performance and minimizing unwanted vibrations and noise.

2.1. Micro-topography generation algorithm based on the conjugate gradient method

The generation of surface micro-topography using the conjugate gradient method primarily entails producing a set of point cloud data with specified statistical distributions for height, followed by the interpolation of a surface representing a rough surface that includes micro-topography. The statistical distribution is characterized by an autocorrelation function, which conveys both the spatial geometric information of the data and the correlations among the data points. The expression for the autocorrelation function of the height values of a three-dimensional rough surface micro-topography is as follows:

$$R(\tau_x,\tau_y)=E\{z(x,y)z(x+\tau_x,y+\tau_y)\} \tag{1}$$

In the expression for the autocorrelation function, $E\{\cdot\}$ represents the mathematical expectation of the random variable. τ_x and τ_y represent the distances of any point in space relative to reference point (x,y) in the x- and y-directions, respectively. $z(x,y)$ and $z(x+\tau_x,y+\tau_y)$ represent the micro-topography height values at points (x,y) and $(x+\tau_x,y+\tau_y)$, respectively. When $x=0$ and $y=0$, $R(0,0)=\sigma^2$, σ represents the arithmetic square root of the height values, which corresponds to the roughness of the three-dimensional surface.

In practical computations, surface micro-topography is often represented via discrete data points. Therefore, the autocorrelation function of the height values is discretized into the following expression:

$$R(\tau_i,\tau_j)=\frac{1}{(N-i)(M-j)}\sum_{k=1}^{N-i}\sum_{l=1}^{M-j}z(x_k,y_l)z(x_k+i\Delta x,y_l+j\Delta y) \tag{2}$$
$$i=0,1,\cdots,n<N;j=0,1,\cdots,m<M$$

where τ_i and τ_j represent the distances in the x and y directions, respectively, of any discrete point relative to the point (x_k,y_l). N and M denote the number of data points in the x and y directions, respectively, whereas Δx and Δy represent the distances between adjacent data points in the x and y directions, respectively. i and j indicate the number of intervals in the x and y directions, respectively, relative to (x_k,y_l), and n and m represent the maximum number of intervals in the x and y directions, respectively. The autocorrelation length of surface micro-topography refers to the distance at which the autocorrelation function value decreases to a critical value v in a specific direction. For isotropic surface micro-topography, the autocorrelation lengths are uniform in all directions, indicating identical statistical properties across all orientations. In contrast, for anisotropic surfaces, the autocorrelation lengths differ depending on the direction. In practical engineering applications, the autocorrelation function of various surface micro-topographies can typically be approximated using an exponential function, with the key variables being the autocorrelation lengths in two mutually perpendicular directions. The exponential function expression used in this study is as follows[25]:

$$R(\tau_x,\tau_y)=\sigma^2\exp\left\{-2.3\cdot\left[\left(\frac{\tau_x}{\beta_x}\right)^2+\left(\frac{\tau_y}{\beta_y}\right)^2\right]^{1/2}\right\} \tag{3}$$

where β_x and β_y represent the autocorrelation lengths in the x and y directions, respectively. Patir et al.[26] generated an $N\times M$ height matrix $[z_{i,j}]$ with Gaussian distribution characteristics, which was very similar to a given autocorrelation function using a linear transformation method. By incorporating the theory of the moving average model, the $N\times M$ height matrix $[z_{i,j}]$ can be obtained from an $(N+n)\times(M+m)$ independent random sequence $[\eta_{i,j}]$ with a standard normal distribution and an $n\times m$ autocorrelation coefficient matrix $[h_{k,l}]$ through the following expression[25]:

$$z_{i,j}=\sum_{k=1}^{n}\sum_{l=1}^{m}h_{k,l}\eta_{i+k,j+l};\quad \begin{matrix}i=1,2,...,N\\ j=1,2,...,M\end{matrix} \tag{4}$$

where $[h_{k,l}]$ is the autocorrelation coefficient matrix solved on the basis of the given autocorrelation function and where $[\eta_{i,j}]$ is an independent random sequence with a standard normal distribution, which needs to meet the following conditions[25]:

$$E(\eta_{i,j}\eta_{k,l})=\begin{cases}1 & \text{if}\quad i=k,j=l\\ 0 & \text{if}\quad \text{otherwise}\end{cases} \tag{5}$$

On the basis of Eqs. (1) and (2), the following expression can be derived[25]:

$$R_{p,q}=E(z_{i,j}z_{i+p,j+q})=\sum_{k=1}^{n-p}\sum_{l=1}^{m-q}h_{k,l}h_{k+p,l+q},p=1,2,...,(n-1),q=1,2,...,(m-1) \tag{6}$$

This expression represents a set of $n\times m$ nonlinear equations, where $[R_{p,q}]$ is the autocorrelation function matrix used to solve the autocorrelation coefficient matrix $[h_{k,l}]$.

This study utilizes the conjugate gradient method to solve the nonlinear equation set, streamlining computations by leveraging differential forms of the equations and obviating the necessity for explicit expressions. Eq.(6) can be rewritten as follows[25]:

$$f'_{i,j}=\sum_{k=1}^{n-p}\sum_{l=1}^{m-q}h_{k,l}h_{k+p,l+q}-R_{p,q} \tag{7}$$

In the conjugate gradient method, the residual is typically set in the negative gradient form.

$$r_{(i)}=-f'_{i,j}(x_{(i)}) \tag{8}$$

where i represents the iteration number. The variable x is updated iteratively through the following expression:

$$x_{(i+1)}=x_{(i)}+\alpha_{(i)}d_{(i)} \tag{9}$$

In the expression, $d_{(i)}$ represents the search direction matrix of the conjugate gradient method, obtained through the Gram-Schmidt method; $\alpha_{(i)}$ represents the parameter that minimizes the equation $f(x_{(i)}+\alpha_{(i)}d_{(i)})$, which converges to the following expression[25]:

$$\alpha=-\varepsilon\frac{[f'(x)]^{\mathrm{T}}d}{[f'(x+\varepsilon d)]^{\mathrm{T}}d-[f'(x)]^{\mathrm{T}}d} \tag{10}$$

In the expression, ε is an arbitrarily small non-zero number. The iterative process for $d_{(i)}$ is as follows[25]:

$$\begin{cases}r_{(i+1)}=-f'(x_{(i+1)})\\ \beta_{(i+1)}=\dfrac{r^T_{(i+1)}(r_{(i+1)}-r_i)}{r^T_{(i)}r_{(i)}}\\ d_{(i+1)}=r_{(i+1)}+\beta_{(i+1)}d_{(i)}\end{cases} \tag{11}$$

During the iterative process, the initial value of the autocorrelation coefficient matrix $[h_{k,l}]$ can be obtained through the following expression[25]:

$$\begin{cases}h^0_{i,j}=kc_{i,j}\\ c_{i,j}=\dfrac{R_{i-1,j-1}}{(n-i+1)(m-j+1)}\\ k^2=\dfrac{R_{0,0}}{\sum_{i=1}^{n}\sum_{j=1}^{m}c^2_{i,j}}\end{cases} \tag{12}$$

Given the global convergence condition ε_{cg}, the solution process converges when $\|r_i\|\leqslant\varepsilon_{cg}\|r_0\|$ or the number of iterations i exceeds the given maximum number of search iterations $i_{\max}$.

By adjusting the autocorrelation lengths β_x and β_y in two directions, it is possible to generate isotropic or anisotropic surfaces with specific textures. Altering σ can control the surface roughness. As shown in Fig. 1(a), a rough surface with autocorrelation length $\beta_x=\beta_y=5$ μm and surface roughness $\sigma=3.2$ μm is presented. In contrast, Fig. 1(b) shows an anisotropic surface with an autocorrelation length $\beta_x=15$ μm in the x-direction, $\beta_y=5$ μmin the y-direction, and a roughness$\sigma=0.5$ μm.

2.2. Micro-topography modeling of tooth profile-modified tooth surfaces

Fig. 2 illustrates the principle of uniformly dividing an involute curve using discrete data points. Point A is the starting point of the involute, Point D is the point at the tip of the tooth, and Point B is the tangent point of the tooth tip generating line with the base circle. The radius of the tooth tip circle is r_a, the pressure angle at the tooth tip is α_a, the length of the tooth tip generating line is p_a, and the radius of the base circle is r_b.

The polar coordinate formula for the involute curve is as follows:

$$\begin{cases}\theta=\tan\alpha-\alpha\\ r=\dfrac{r_b}{\cos\alpha}\end{cases} \tag{13}$$

where θ is the polar angle, r is the polar radius, r_b is the radius of the base circle, and α is the pressure angle at a certain point on the involute. The arc length differential is

$$\mathrm{d}s=\sqrt{r^2+r'^2}\,\mathrm{d}\theta=r_b\tan\alpha\mathrm{d}\tan\alpha \tag{14}$$

Let the arc length from point i to point $i+1$ on the involute be denoted as s; then, s can be expressed as

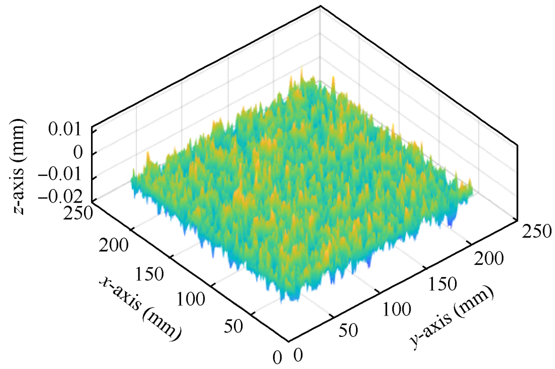

(a) $\beta_x=\beta_y=5$ μm, $\sigma=3.2$ μm

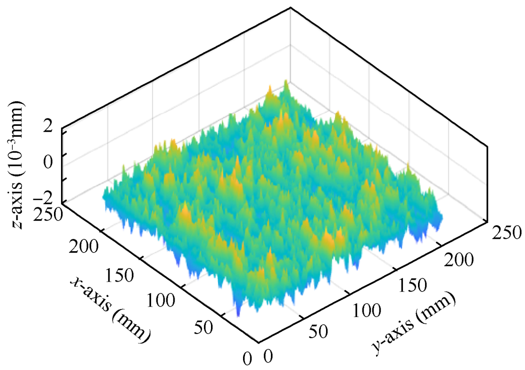

(b) $\beta_x=15$ μm, $\beta_y=15$ μm, $\sigma=0.5$ μm

Fig. 1. Isotropic and anisotropic surfaces under different roughness conditions.

$$\begin{aligned} s &= \int_{\alpha_i}^{\alpha_{i+1}} r_b \tan\alpha \mathrm{d} \tan\alpha \\ &= \frac{1}{2} r_b (\tan^2\alpha_{i+1} - \tan^2\alpha_i) \end{aligned} \tag{15}$$

The involute discretization process involves substituting chord length for arc length between adjacent points on the involute and can be represented as

$$f \approx s = \frac{r_b}{2}(\tan^2\alpha_{i+1} - \tan^2\alpha_i) \tag{16}$$

Given the pressure angle α_i at point i, the pressure angle α_{i+1} at point $i+1$ can be obtained through the following formula:

$$\alpha_{i+1} = \mathrm{a}\tan\left(\sqrt{\tan^2\alpha_i + \frac{2f}{r_b}}\right) \tag{17}$$

The polar radius at point i can be expressed as

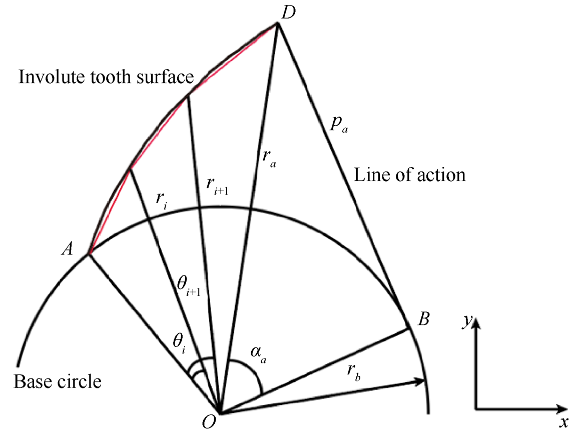

Fig. 2. Uniform division of the involute curve using discrete data points.

$$r_i = \frac{r_b}{\cos\alpha_i} \tag{18}$$

The length of the generating line at point i can be expressed as

$$p_i = r_b \tan\alpha_i \tag{19}$$

Combining Eqs. (13) and (17), if the (r,θ) coordinates of a node are known, the (r,θ) coordinates of the next node on the involute can be determined. By applying coordinate transformation, the polar coordinates of the nodes are converted to Cartesian coordinates. Subsequently, knowing the Cartesian coordinates of all discrete nodes forming the involute in the x-y plane enables the creation of an ideal involute tooth surface with a uniform grid by extrapolating these nodes along the z-direction.

The ideal involute tooth surface, modeled using a uniform grid, can undergo modification based on tooth profile modification theory. Fig. 3 illustrates that the modification amount at any point on the tooth profile, in the direction of the generating line, is defined by parameters including maximum relief magnitude (C_T at the tip and C_B at the root), modification length (L_T at the tip and L_B at the root), and modification curve characteristics (typically comprising straight lines and parabolas). The modification amount at any point on the tooth profile can be expressed as

$$\begin{cases} e^T(p_i) = C_T\left(\dfrac{(p_i - p_i^c)}{L_T}\right)^n & n=1,2; \quad p_i \in [p_i^c, p_i^d] \\ e^B(p_i) = C_B\left(\dfrac{(p_i^b - p_i)}{L_B}\right)^n & n=1,2; \quad p_i \in [p_i^a, p_i^b] \end{cases} \tag{20}$$

where $e^T(p_i)$ and $e^B(p_i)$ represent the magnitude of the tip and root relief at any point on the tooth profile, respectively; p_i^b and p_i^c denote the modification lengths corresponding to the upper and lower

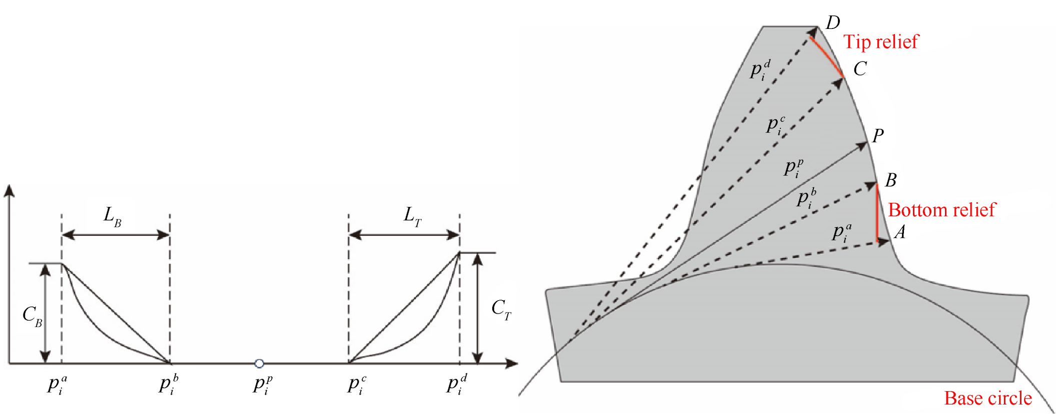

Fig. 3. Tooth profile modification method.

boundary points in the single-tooth engagement zone, respectively. p_i represents the modification length at any point on the tooth profile. n indicates the exponent of the modification curve; when n = 1, it represents linear modification, and when n = 2, it represents parabolic modification.

This study exclusively implements tooth tip modification on the driving and driven gears. By subsequently integrating Eqs. (18), (19), and (20), the geometric parameters of individual points on the modified gear tooth surfaces can be computed:

$$\begin{cases} p'_{i,j}=p_{i,j}-e^{T}_{i,j}(p_i) \\ r'_{i,j}=\sqrt{{p'_{i,j}}^2+r_b^2} \\ \alpha'_{i,j}=a\tan(\frac{p'_{i,j}}{r'_{i,j}}) \end{cases} \tag{21}$$

where $p_{i,j}$ represents the generating line length of any point on the involute tooth surface; $e^{T}_{i,j}(p_i)$ denotes the tooth tip modification amount at any point on the involute tooth surface; and $p'_{i,j}$, $r'_{i,j}$, and $\alpha'_{i,j}$ are the generating line length, polar radius, and pressure angle of any point on the modified tooth surface, respectively.

Subsequently, by superimposing the surface micro-topography height information generated in Section 1.1 onto the corresponding data points of the ideal modified tooth surface, a modified tooth surface that takes micro-topography into account can be obtained. This process can be represented as

$$\begin{cases} p''_{i,j}=p'_{i,j}+z_{i,j} \\ r''_{i,j}=\sqrt{{p''_{i,j}}^2+r_b^2} \\ \alpha''_{i,j}=a\tan(\frac{p''_{i,j}}{r''_{i,j}}) \end{cases} \tag{22}$$

where $p''_{i,j}$, $r''_{i,j}$, and $\alpha''_{i,j}$ represent the generating line length, polar radius, and pressure angle, respectively, of any point on the modified tooth surface after considering the micro-topography. The process of tooth profile modification on the involute tooth surface and the superposition of surface micro-topography are illustrated in Fig. 4.

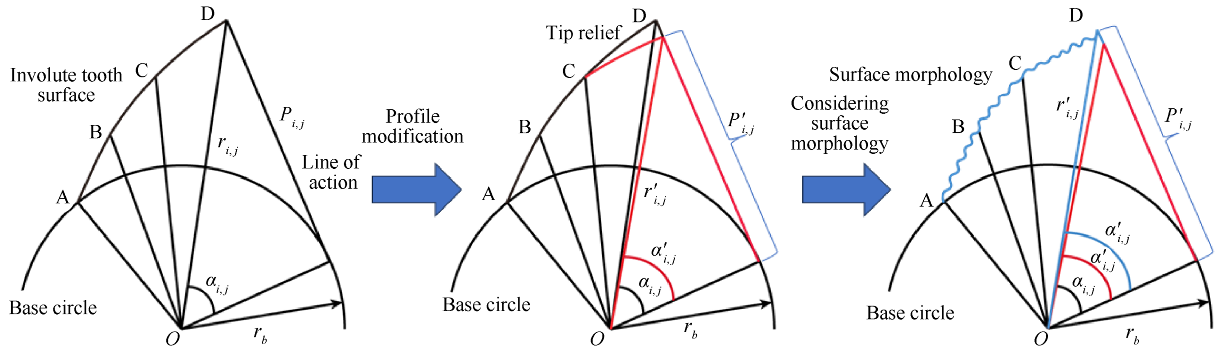

Fig. 4. Tooth profile modification and superposition of the surface micro-topography.

The process described above was implemented in MATLAB to model the modified tooth surface while considering micro-topography, and the results are shown in Fig. 5.

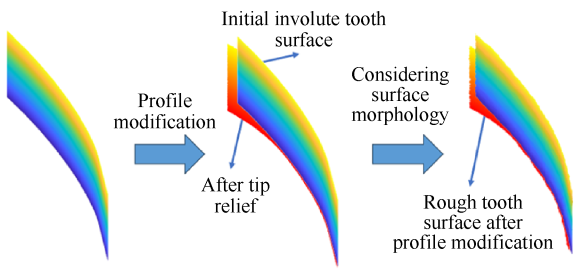

Fig. 5. Modeling process of a modified tooth surface considering micro-topography.

3. Finite element modeling of modified gears and dynamic simulation of the meshing process

Finite element meshing of gears with rough modified tooth surfaces is performed utilizing the commercial pre-processing software Hypermesh 12.0. The mesh density varies, with finer meshes on the tooth surfaces and coarser meshes in regions farther away from the surfaces. A three-tooth finite element model, comprising 252516 meshes, is established as shown in Fig. 6(a). A paired meshing gear finite element model is constructed, illustrated in Fig. 6(b), where the driving gear undergoes counter-clockwise rotation and the driven gear undergoes clockwise rotation. Each tooth of both the driving and driven gears is uniquely numbered. The gear parameters are summarized in Table 1.

The finite-element model parameters are subsequently defined. The mesh element type is specified as SOLID185. Structural steel is designated as the gear material, with material parameters provided in Table 2. The tooth surface contact is modeled as frictional contact, with a friction coefficient of 0.05. The meshing surfaces of the three teeth of the driven gear are designated as contact surfaces, while the corresponding surfaces of the driving gear are designated as target surfaces. The contact and target surfaces are discretized using CONTA173 and TARGE170 elements, respectively.

Boundary conditions are applied as follows: rotational pairs are defined on the spoke surfaces of both the driving and driven gears, allowing rotation around the z-axis. The spoke surfaces are considered rigid, with all degrees of freedom constrained except for ROTZ. The finite-element model is then imported into Ansys Workbench, where kinematic pair loads are applied within the transient dynamics module. Specifically, the driving gear is subjected to a counter-clockwise rotational speed load, comprising an initial acceleration phase followed by uniform speed rotation throughout one meshing cycle. Conversely, the driven gear is loaded with a counter-clockwise torque, applied via a ramp function, which increases linearly during acceleration and remains constant during uniform rotation.

The analysis settings are then configured. The entire analysis process is divided into five load steps, as illustrated in Fig. 7. The first load step addresses the acceleration phase and the torque loading process (from position 0 to position 1). Upon completion of this step, the gears begin meshing, followed by rotation at a uniform speed. The second load step involves the double-tooth meshing pro-

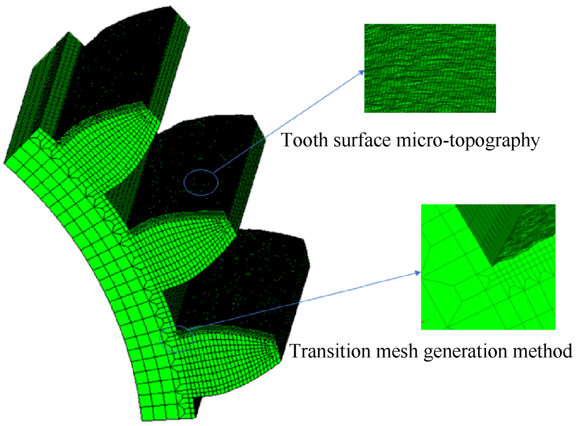

(a) Three-tooth finite element model

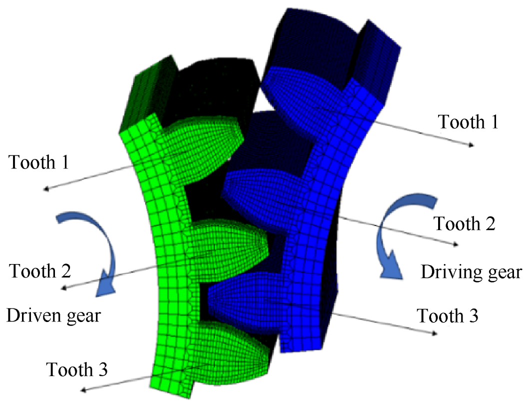

(b) Finite element model of meshing gears

Fig. 6. Finite element modeling of the meshing process of modified gears.

Table 1 Geometric parameters of gears.

Parameters	Driving gear	Driven gear
Number of teeth	25	25
Module (mm)	3	3
Pressure angle (°)	20	20
Tooth width (mm)	20	20
Addendum coefficient	1	1
Clearance coefficient	0.25	0.25

Table 2 Gear material parameters.

Parameters	Structural steel
Young's modulus (GPa)	200
Poisson's ratio	0.3
Density ($kg \cdot m^{-3}$)	7850

cess, during which the first and second teeth of the driving and driven gears bear the load. At the end of this step, the gears transition from double-tooth to single-tooth meshing. The third and fourth load steps represent the single-tooth meshing processes. Upon the completion of the third load step, the gears reach the nodal meshing position, and following the fourth load step, the gears transition back to double-tooth meshing. The fifth load step involves another double-tooth meshing process, where the second and third teeth of both the driving and driven gears carry the load. Upon the completion of all load steps, the dynamic simulation of a complete meshing cycle at a specific rotational speed is achieved.

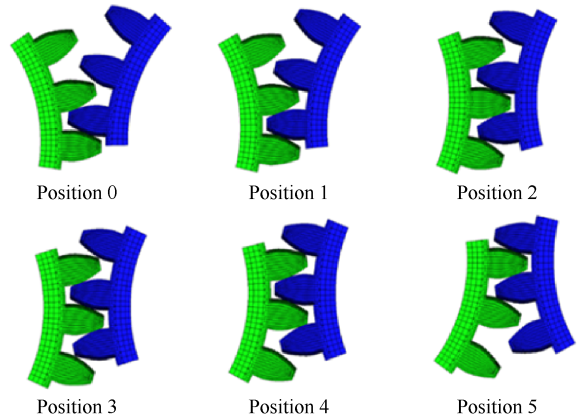

Fig. 7. Dynamic simulation of the gear meshing process.

After the dynamic simulation of the gear meshing process is completed, the rotation angles of the driving gear and the driven gear can be obtained at any time during the entire meshing process. The rotation angle of the driving gear at any time is denoted as θ_1, and the rotation angle of the driven gear at any time is denoted as θ_2. The static transmission error (STE) of the gear mechanism can be defined as the angular difference between the theoretical meshing position and the actual meshing position of the driven gear and can be calculated via the following formula:

$$\mathrm{STE} = r_{B1}\theta_1 - r_{B2}\theta_2 \tag{23}$$

where r_{B1} and r_{B2} are the base circle radii of the driving gear and the driven gear, respectively. The peak-to-peak static transmission error (PPSTE) is considered an important indicator for measuring the vibration and noise of the gear mechanism and can be calculated via the following formula:

$$\mathrm{PPSTE} = \max(\mathrm{STE}) - \min(\mathrm{STE}) \tag{24}$$

4. Blending ensemble learning and differential evolution optimization algorithm

4.1. Blending ensemble learning strategy

The concept of the Blending ensemble learning model originated from the strong demand in the field of machine learning to improve the performance of predictive models. In the Netflix Prize competition, researchers have reported that the predictive ability of a single model is limited and that combining multiple models can significantly enhance the predictive performance. This led to the proposal of the Blending ensemble learning strategy, whose process is illustrated in Fig. 8.

This process can be divided into the following steps:

(1) Data partitioning

The original dataset is partitioned into a training set and a test set according to a certain ratio, and then the training set is further divided into a validation set.

(2) Base learner construction and training

Multiple different types of base models, such as decision trees, support vector machines, and neural networks, are selected. Considering the correlation of errors and the predictive performance of the models, the optimal models are chosen as the base learners of the ensemble learning model. Then, the newly partitioned training set (excluding the validation set) is used to train each base learner individually and predict on the validation set.

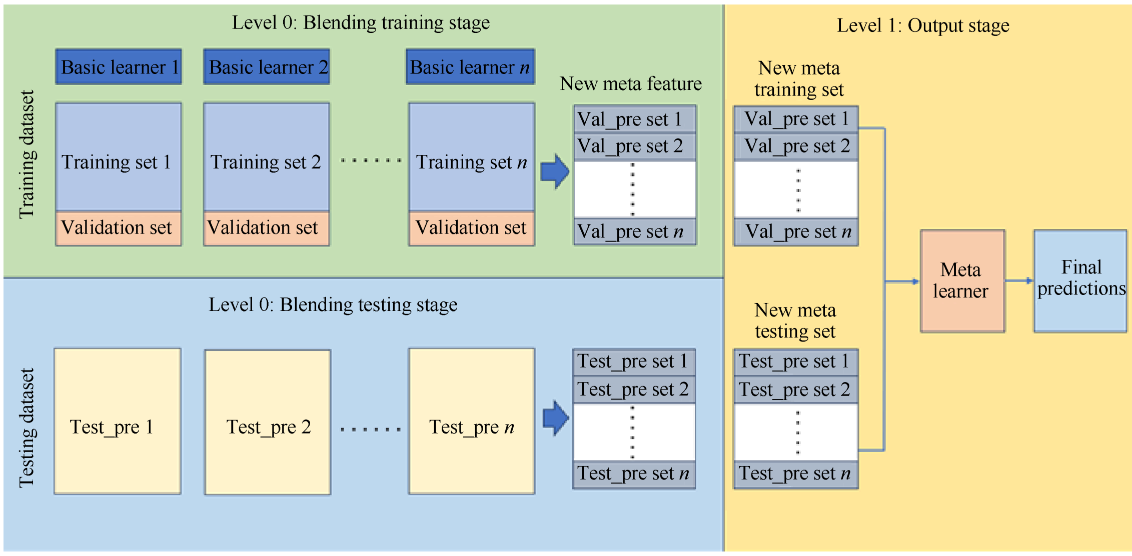

Fig. 8. Blending ensemble learning framework.

(3) Meta-learner construction and training

Combine the prediction results of each base learner on the validation set as meta-features with the true labels of the validation set to construct a new dataset, which is called the meta-dataset. The inputs of the meta-dataset are the meta-features, and the outputs are the true labels of the validation set. One or more meta-models are selected, and the constructed meta-dataset is used to train the meta-models.

(4) Model evaluation and integration

The test set is used to evaluate the entire ensemble model (including base learners and meta-learners), and the meta-model with the highest prediction accuracy is selected as the meta-learner of the ensemble learning model. The base learners predict on the test set to obtain meta-features, and the meta-learner makes the final prediction on the test set on the basis of these meta-features. Evaluate the performance of the ensemble model by calculating evaluation metrics such as the mean squared error (MSE), mean absolute error (MAE), and mean absolute percentage error (MAPE).

4.2. Selection of learners in the blending ensemble learning model

The predictive performance of the Blending ensemble learning model depends on the predictive performance of single models and the combined predictive effect of different models. The stronger the learning ability of a single model and the greater the algorithmic difference between different models, the better the predictive performance of the ensemble learning model. It is necessary to comprehensively consider the model differences and prediction accuracy while selecting several models as the base learners and meta-learners of the Blending ensemble learning model. The selection method is as follows:

(1) First, the Pearson correlation coefficient is used to calculate the degree of error difference for each model. The calculation method is as follows:

$$P_{xy}=\frac{\sum_{m}^{i=1}(x_i-\bar{x})(y-\bar{y})}{\sqrt{\sum_{m}^{i=1}(x_i-\bar{x})^2}\sqrt{\sum_{m}^{i=1}(y_i-\bar{y})^2}} \tag{25}$$

In the formula, x_i and y_i represent the elements of each model vector, and $\bar{x}$ and $\bar{y}$ are the average values of the elements in each vector. According to the Pearson correlation coefficient, the Pearson correlation diagrams of each model are drawn to determine several models with the highest error correlation, and then the model with the lowest mean absolute percentage error (MAPE) is selected as one of the base learners of the ensemble learning model.

(2) Among the remaining models with relatively low error correlations, several models with the lowest mean absolute percentage error (MAPE) are selected as the other base learners of the ensemble learning model.

(3) Several models are used as meta-learners of the ensemble learning model for training, the mean absolute percentage error of the ensemble learning model prediction under each meta-learner is compared, and the meta-learner with the highest prediction accuracy is selected.

4.3. Differential evolution algorithm

The differential evolution (DE) algorithm is a population-based heuristic search algorithm for solving continuous optimization problems. It was proposed by Rainer Storn and Kenneth Price in 1995. Inspired by the genetic algorithm, it adopts unique mutation and crossover mechanisms. The overall process of the differential evolution algorithm is shown in Fig. 9, which mainly includes the following five steps:

(1) Initialize the population as $\{X_i(0)|x_{i,j}^L\leqslant x_{i,j}(0)\leqslant x_{i,j}^U; i=1,2,\cdots,\mathrm{NP}\ j=1,2,\cdots,D\}$ and then randomly generate each population individual via the following formula:

$$x_{i,j}(0)=x_{i,j}^L+\mathrm{rand}(0,1)\cdot\left(x_{i,j}^U-x_{i,j}^L\right) \tag{26}$$

where $X_i(0)$ represents the i-th individual in the 0-th generation of the population, $x_{i,j}(0)$ represents the j-th gene of the i-th individual in the 0-th generation, NP represents the population size, and rand(0,1) represents a random number uniformly distributed in the interval (0, 1).

(2) Mutation: The mutation operation is a crucial component of the differential evolution algorithm, facilitating individual diversification through differential operations. This process involves randomly selecting two distinct individuals from the population and computing their vector difference. The resulting difference is then scaled and combined with the target individual to be mutated. Several differential strategies are commonly employed, including:

$$v_i(g+1)=x_{i_1}(g)+F\cdot(x_i(g)-x_{ij}(g))$$
$$i\neq r_1\neq r_2\neq r_3 \tag{27}$$

In the formula, F is the scaling factor, and $x_i(g)$ is the i-th individual in the g-th generation population. During the evolution process, the validity of the newly generated solutions must also be ensured. Therefore, it is necessary to determine whether the generated solutions meet the boundary conditions. If not, they need to be regenerated. The g-th generation population can be represented as

$$\{x_i(g)|x^L_{i,j}\leqslant x_{j,i}(g)\leqslant x^v_{i,j}, i=1,2,\cdots,\mathrm{NP}; j=1,2,\cdots,D\} \tag{28}$$

The mutated g-th generation population can be represented as

$$\{x_i(g+1)|x^L_{i,j}\leqslant x_{j,i}(g+1)\leqslant x^v_{i,j}, i=1,2,\cdots,\mathrm{NP}; j=1,2,\cdots,D\} \tag{29}$$

(3) Crossover: The g-th generation population and the mutated intermediates are used for crossover. This process can be represented as

$$u_{i,j}(g+1)=\begin{cases} v_{i,j}(g+1) & \text{if } \mathrm{rand}(0,1)\leqslant \mathrm{CR} \text{ or } j=j_{\mathrm{rand}} \\ x_{i,j}(g) & \text{otherwise} \end{cases} \tag{30}$$

where CR represents the crossover probability and where j_{rand} represents a random integer.

(4) Selection: The greedy algorithm is used to select the population individuals for the next generation. This process can be represented as

$$x_i(g+1)=\begin{cases} u_i(g+1) & \text{if } f(u_i(g+1))\leqslant f(x_i(g)) \\ x_i(g) & \text{otherwise} \end{cases} \tag{31}$$

(5) Termination conditions: Repeat steps 2 to 4 until a certain termination condition is met, such as reaching the maximum number of iterations or the quality of the solution reaching a predetermined threshold.

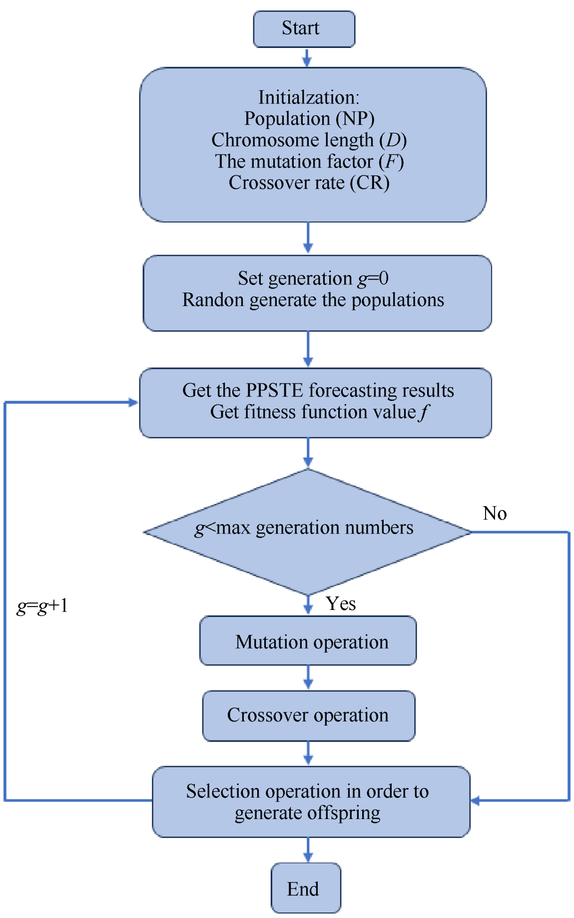

Fig. 9. Overall process of the differential evolution algorithm.

5. Prediction of the gear static transmission error peak-to-peak value and optimization of tooth profile modification

5.1. Dataset generation and surrogate model selection

The modification parameters include the maximum modification amounts at the tooth tips of the driving and driven wheels, C_{T1} and C_{T2}, and the modification lengths of the driving and driven wheels, L_{T1} and L_{T2}. The range of the former is 0 μm to 18 μm, and the range of the latter is 2.7085 mm to 5.417 mm. The Latin hypercube sampling (LHS) method is used to randomly generate 50 sets of modification parameters. According to the modeling method in Chapter 3, 50 sets of modified driving and driven gears are constructed. The geometric and material parameters of the gears are shown in Tables 1 and 2. The tooth surface roughness of the driving and driven wheels is set to Ra0.5 and Ra3.2, respectively. Under the working condition that the load of the driven wheel is 100 N·m, the meshing processes of the 50 sets of modified gears are simulated via the finite element method, and the peak-to-peak values of the static transmission errors of each set of modified gears are calculated. Finally, a dataset of 50 sets of data is obtained. The dataset is divided into a training set and a test set at a ratio of 8:2, and then the training set is divided into a new training set and a validation set again at a ratio of 8:2.

Eight surrogate models, including random forest (RF), support vector regression (SVR), the radial basis function (RBF), the gradient boosting machine (GBM), CatBoost, XGBoost, AdaBoost, and Extra-Trees Regressor are selected. We train them on the new training set and then calculate the mean absolute error (MAE), root mean square error (RSME), and mean absolute percentage error (MAPE) of the test set data. The calculation formulas are as follows:

$$\mathrm{MAE}=\frac{1}{n}\sum_{n}^{i=1}|y_i-\hat{y}_i| \tag{32}$$

$$\mathrm{RMSE}=\sqrt{\frac{1}{n}\sum_{i=1}^{n}(y_i-\hat{y}_i)^2} \tag{33}$$

$$\mathrm{MAPE}=\frac{100\%}{n}\sum_{n}^{i=1}\left|\frac{\hat{y}_i-y_i}{y_i}\right| \tag{34}$$

In the formula, n is the number of samples, $\hat{y}_i$ is the predicted value of the peak-to-peak value of the static transmission error, and y_i is the true value of the peak-to-peak value of the static transmission error.

5.2. Prediction of the peak-to-peak value of the static transmission error based on blending ensemble learning

To construct a Blending ensemble learning model with the highest prediction accuracy, it is necessary to comprehensively consider the prediction accuracy and differences among the abovementioned eight single surrogate models and preferably select four base learners and one meta-learner. The prediction accuracies of these eight surrogate models are shown in Table 3. The prediction performances of various models vary greatly. For example, when the MAPE is taken as the evaluation index, the accuracy of the RBF is the highest, whereas the accuracies of XGBoost and the GBM are relatively low. When selecting the base learners of the Blending ensemble-learning model, not only the prediction accuracy of a single model but also the algorithm differences between different models should be considered. The Pearson correlation coefficient is used as the correlation index to calculate the error differences of each model and draw the Pearson correlation diagram. The error correlations of each model are shown in Fig. 10.

Table 3 Prediction results of single surrogate models.

Meta-model	RSME (μm)	MAE (μm)	MAPE
RF	0.876	0.726	15.968%
SVR	0.855	0.697	14.630%
RBF	0.840	0.696	14.401%
ETR	0.920	0.787	16.893%
GBM	1.108	0.905	20.864%
CatBoost	1.024	0.770	16.535%
XGBoost	1.046	0.864	19.906%
AdaBoost	0.890	0.742	16.292%

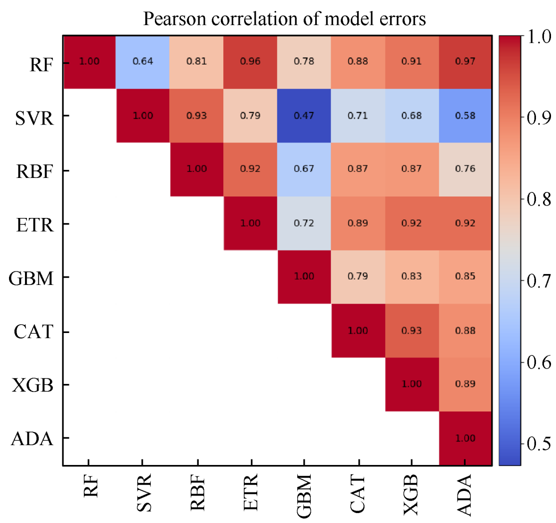

Fig. 10 Pearson correlation diagram.

The figure shows that the error correlations of the RF (Random Forest), ETR (Extra-Trees Regressor), and ADA (AdaBoost) models are relatively high. Selecting these three models simultaneously as base learners for Blending ensemble learning increases the overfitting risk. Therefore, among these three, the RF with the smallest mean absolute percentage error (MAPE) is selected as one of the base learners. Among the remaining five models with relatively low error correlations, three models with the lowest error correlations with the GBM are selected: support vector regression (SVR), gradient boosting machine (GBM), and radial basis function (RBF) as the other three base learners.

Each of the above eight single models is used as a meta-learner for Blending ensemble learning. The mean absolute error (MAE), root mean square error (RSME), and MAPE of different meta-learners are shown in Table 4. The table shows that when the RBF is used as the meta-learner of the Blending ensemble learning model, all the error indicators of the model are the lowest, and the MAPE is only 14.183%.

In summary, the base learners used in Blending ensemble learning are RF, SVR, GBM, and RBF, and the meta-learner is RBF. Compared with those of the single models, the prediction errors of the Blending ensemble learning model are lower, with an average decrease of 2.75%, which proves the accuracy and reliability of the adopted Blending ensemble learning method.

Table 4 Evaluation indicators of the meta-learners.

Meta-model	RSME (μm)	MAE (μm)	MAPE
RF	0.813	0.670	14.559%
SVR	1.073	0.8	17.025%
RBF	0.880	0.663	14.183%
ETR	0.950	0.705	15.143%
GBM	0.853	0.709	16.024%
CatBoost	0.821	0.675	14.729%
XGBoost	1.046	0.864	19.906%
AdaBoost	0.898	0.809	18.214%

5.3. Optimization of tooth profile modification for spur gears

Based on the Blending ensemble-learning model exhibiting the highest prediction accuracy in Section 5.2, which targets the minimization of the peak-to-peak value of gear static transmission error, the differential evolution algorithm outlined in Section 3.3 is utilized to optimize modification parameters. The optimization algorithm's parameters are set as follows: maximum iterations at 1000, population size at 30, scaling factor F determined by the mutation parameter with a range of (0.5, 1), crossover probability CR at 0.7, and convergence tolerance at 0.01. The optimized modification parameters for the driving and driven wheels are presented in Table 5.

Table 5 Optimal gear modification parameters.

Type	Addendum modification amount C_T (μm)	Modification length L_T (mm)
Driving gear	2.736	4.454
Driven gear	4.15	3.57

To prove the accuracy of the optimization results, four sets of modification parameters were randomly generated. The meshing processes of the four sets of modified gears were modeled and simulated, and the peak-to-peak static transmission error (PPSTE) was calculated and compared with that of the optimal modification parameters. The modification parameters and the corresponding PPSTE values are shown in Table 6, and the static transmission error curves are shown in Fig. 11. The gear pair optimized with the modified parameters exhibits the minimal fluctuation in static transmission error, with a peak-to-peak value (PPSTE) of merely 3.69 μm. A comparative analysis with four additional gear pair sets featuring randomly modified parameters reveals an average reduction of 23.19% in PPSTE. This notable decrease demonstrates a substantial enhancement in the vibration and noise reduction capabilities of the gear pair, thereby validating the efficacy and reliability of the proposed methodology in this study.

Table 6 Comparison between randomly generated modification parameters and optimization results.

Group number	C_T(μm)	L_T(mm)	C_T(μm)	L_T(mm)	PPSTE(μm)
1	1.163	4.681	3.23	5.329	5.535
2	11.129	4.783	17.351	3.274	4.674
3	13.792	4.232	15.013	3.059	4.613
4	5.445	4.394	0.14	4.125	4.305
Optimization results	2.736	4.454	4.15	3.57	3.69

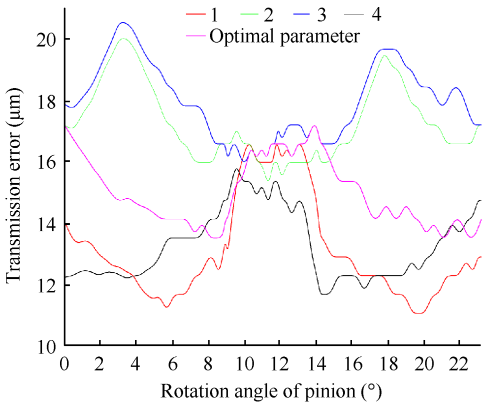

Fig. 11 Static transmission errors of gear pairs with random modification parameters and optimal modification parameters.

6. Conclusions

In this work, under the condition of considering the micro-topography of the tooth surface and the micro-contact in the meshing process, a surrogate model for predicting gear transmission error was established, and the tooth profile modification parameters were optimized and verified. The following conclusions were obtained:

(1) A modeling method for the modified tooth surface considering the micro-topography and a simulation method for the meshing process of the modified gear under micro-contact conditions are proposed. On the basis of the conjugate gradient method, the micro-topography of the tooth surface is generated, and a modified gear model considering the micro-topography is established. The meshing process simulation under the micro-contact condition is realized, the static transmission error curve is accurately drawn, and the peak-to-peak value of the static transmission error is calculated as a quantitative index of the static transmission error.

(2) A Blending ensemble learning model for predicting the peak-to-peak value of the static transmission error of the modified gear was constructed. The finite element method was used to construct the dataset and train eight single surrogate models. Taking the mean absolute percentage error (MAPE) as the evaluation index, an ensemble learning model with random forest (RF), support vector regression (SVR), gradient boosting machine (GBM), and radial basis function (RBF) as base learners and an RBF as a meta-learner was constructed, and the MAPE was only 14.183%. Compared with that of the single model, the prediction error of the Blending ensemble learning model decreased by an average of 2.75%.

(3) This study determines the optimal modification parameters that minimize the peak-to-peak value of gear static transmission error under micro-contact conditions. Utilizing the differential evolution algorithm, the Blending ensemble learning model is optimized with the minimization of peak-to-peak static transmission error as its objective. The resulting optimal modification parameters, verified through finite element analysis, yield a peak-to-peak value of gear static transmission error of only 3.69 μm. This represents an average reduction of 23.19% compared to gear pairs with randomly generated modification parameters.

Acknowledgements

This study was supported by the National Defense Basic Research Project (No. JCKY2022203C024).

References

1. YANG JX, CHEN ZY, SHI WK, et al. Vibration control of commercial vehicle drive axles based on modification of helical gears. *Mechanical Systems and Signal Processing* 2023; 193:110252.
2. HOTAIT M A, KAHRAMAN A. Experiments on the relationship between the dynamic transmission error and the dynamic stress factor of spur gear pairs. *Mechanism and Machine Theory* 2013; 70: 116-128.
3. PALERMO A, BRITTE L, JANSSENS K, et al. The measurement of gear transmission error as an NVH indicator: Theoretical discussion and industrial application via low-cost digital encoders to an all-electric vehicle gearbox. *Mechanical Systems and Signal Processing* 2018; 110: 368-389.
4. Zhou Y, Hong LF, Li XY, et al. Investigation on transient dynamics of rotor system in air turbine starter based on magnetic reduction gear. *Journal of Advanced Manufacturing Science and Technology* 2021; 1 (3): 2021009.
5. Zhao WS, Guo Q, Shu CL, et al. Methods on error-modeling, detection and compensation in gear hobbing process: A short review. *Journal of Advanced Manufacturing Science and Technology* 2023; 3(1): 2022019.
6. Liu D, Shi J, Liao ZR, et al. Prognostics and health management for electromechanical system: A review. *Journal of Advanced Manufacturing Science and Technology*. 2022; 2(4):2022015.
7. Zeng ZW, Miao Q. Simulation and analysis of hydraulic driven faults in rotating airplane cabin doors. *Journal of Advanced Manufacturing Science and Technology*. 2023;3(4):2023014.
8. Feng K, Ni Q, Beer M, et al. A novel similarity-based status characterization methodology for gear surface wear propagation monitoring. *Tribology International* 2022; 174: 107765.
9. Mounir H, Nizar A, Abdelmajid B. CAD model simplification using a removing details and merging faces technique for a FEM simulation. *Journal of Mechanical Science and Technology* 2012; 26: 3539-3548.
10. Lakshmi Narayana A, Rao K, Vijaya Kumar R. FEM buckling analysis of quasi-isotropic symmetrically laminated rectangular composite plates with a square/rectangular cutout. *Journal of Mechanical Science and Technology* 2013; 27: 1427-1435.
11. Zhou YH, Sun H, Li AH, et al. FEM simulation-based cutting parameters optimization in machining aluminum-silicon piston alloy ZL109 with PCD tool. *Journal of Mechanical Science and Technology* 2019; 33: 3457-3465.
12. Wu YJ, Wang JJ, Han QK. Static/dynamic contact FEA and experimental study for tooth profile modification of helical gears. *Journal of Mechanical Science and Technology* 2012; 26: 1409-1417.
13. Mei WJ, Na JZ, Yang F, et al. The optimal design method and standardized mathematical model of tooth profile modification of spur gear. *Mathematical Problems in Engineering* 2016; 1: 6347987.
14. Chen MZ, Xiong XS, Zhuang WH. Design and simulation of meshing performance of modified straight bevel gears. *Metals* 2020; 11(1): 33.
15. Bellary S, Husain A, Samad A. Effectiveness of meta-models for multi-objective optimization of centrifugal impeller. *Journal of Mechanical Science and Technology* 2014; 28: 4947-4957.
16. Mi L, Yin GF, Sun MN, et al. Effects of preloads on joints on dynamic stiffness of a whole machine tool structure. *Journal of Mechanical Science and Technology* 2012; 26: 495-508.
17. Zhu X, Ran Y, Li XT. Reliability assessment method based on the meta-action unit for complex mechanical system. *Journal of Mechanical Science and Technology* 2023; 37(3): 1233-1242.
18. Li Q, Zhang S, Ma L, et al. Stiffness and damping coefficients for journal bearing using the 3D transient flow calculation. *Journal of Mechanical Science and Technology* 2017; 31: 2083-2091.
19. Korta JA, Mundo D. Multi-objective micro-geometry optimization of gear tooth supported by response surface methodology. *Mechanism and Machine Theory* 2017; 109: 278-295.
20. Mohammed OD, Bhat ADS, Falk P. Robust multi-objective optimiza-

tion of gear microgeometry design. *Simulation Modelling Practice and Theory* 2022; 119: 102593.

21. Liu S, Li B, Gan R, et al. Multi-objective optimization of two-stage helical pairs in helical hydraulic rotary actuator using ensemble of metamodels and NSGA-II. *Actuators* 2023; 12(10): 385.
22. Wang ZR, Huang HA, Wang YR. Fault diagnosis of planetary gearbox using multi-criteria feature selection and heterogeneous ensemble learning classification. *Measurement* 2021; 173: 108654.
23. Bae SM, Seo KJ, Kim DE. Effect of friction on the contact stress of a coated polymer gear. *Friction* 2020; 8: 1169-1177.
24. Roda-Casanova V, Gonzalez-Perez I. Investigation of the effect of contact pattern design on the mechanical and thermal behaviors of plastic-steel helical gear drives. *Mechanism and Machine Theory* 2021; 164: 104401.
25. Liu H, Liu H, Zhu C, et al. Study on gear contact fatigue failure competition mechanism considering tooth wear evolution. *Tribology International* 2020;147: 106277.
26. Zhao Z, Han H, Wang P, et al. An improved model for meshing characteristics analysis of spur gears considering fractal surface contact and friction. *Mechanism and Machine Theory* 2021; 158: 104219.
27. Kubiak KJ, Wilson MCT, Mathia TG, et al. Wettability versus roughness of engineering surfaces. *Wear* 2011; 271(3-4): 523-528.
28. Bakolas V. Numerical generation of arbitrarily oriented non-Gaussian three-dimensional rough surfaces. *Wear* 2003; 254(5-6): 546-554.
29. Patir N. A numerical procedure for random generation of rough surfaces. *Wear* 1978; 47(2): 263-277.